Climatology of Wind-Seas and Swells in the China Seas from Wave Hindcast

QIAN Chengcheng[1), 2), 3)], JIANG Haoyu[2), 4), *], WANG Xuan[5)], and CHEN Ge[2), 3)]

1) *North China Sea Marine Forecasting Center of State Oceanic Administration, Qingdao 266100, China*
2) *Laboratory for Regional Oceanography and Numerical Modeling, Qingdao National Laboratory for Marine Science and Technology, Qingdao 266000, China*
3) *College of Information Science and Engineering, Ocean University of China, Qingdao 266100, China*
4) *College of Marine Science and Technology, China University of Geosciences, Wuhan 430000, China*
5) *College of Ocean Science and Engineering, Shanghai Maritime University, Shanghai 200000, China*

Abstract The wind-sea and swell climates in the China Seas are investigated by using the 27-yr Integrated Ocean Waves for Geophysical and other Applications (IOWAGA) hindcast data. A comparison is made between the significant wave height from the IOWAGA hindcasts and that from a jointly calibrated altimetry dataset, showing the good performance of the IOWAGA hindcasts in the China Seas. A simple but practical method of diagnosing whether the sea state is wind-sea-dominant or swell-dominant is proposed based on spectral partitioning. Different from the characteristics of wind-seas and swells in the open ocean, the wave fields in the enclosed seas such as the China Seas are predominated by wind-sea events in respect of both frequencies of occurrences and energy weights, due to the island sheltering and limited fetches. The energy weights of wind-seas in a given location is usually more significant than the occurrence probability of wind-sea-dominated events, as the wave energy is higher in the wind-sea events than in the swell events on average and extreme wave heights are mostly related to wind-seas. The most energetic swells in the China Seas (and other enclosed seas) are 'local swells', having just propagated out of their generation areas. However, the swells coming from the West Pacific also play an important role in the wave climate of the China Seas, which can only be revealed by partitioning different swell systems in the wave spectra as the energy of them is significantly less than the 'local swells'.

Key words the China Seas; wind-sea; swell; wave climate; WAVEWATCH III

1 Introduction

Wind-generated surface gravity waves (hereinafter, simply called waves) are a ubiquitous phenomenon at the interface between atmosphere and ocean. Although waves are generated by the wind at the sea surface, they are not always coupled to the local wind as they can be further classified into two types: wind-seas and swells. Wind-seas are waves under growth or in equilibrium with the local wind while swells are generally regarded as waves which are not, or hardly, affected by the local wind. Swells are generated when waves propagate out of their generation area or when local wind diminishes or changes its direction (Kinsman, 1965). It is noted that there is no definite boundary between wind-seas and swells as wind-seas will turn into swells in a gradual process. However, some rules of thumb are often used to identify wind-seas and swells roughly. For instance, some thresholds of wave period (usually 10 s) or wave age (usually 1 or 1.2) may be selec-

ted as criteria (*e.g.*, Kinsman, 1965; Drennan *et al.*, 2003).

The purposes and concerns are different in the studies on wind-seas and swells. The studies on wind-seas mainly focus on the generation and growing processes while those of swells mainly focus on their propagation and the impacts on ocean/coastal engineering (*e.g.*, Janssen, 1989; Ardhuin *et al.*, 2009). Therefore, the wave climate community sometimes studies wind-seas and swells separately. Many studies on global or basin-scale wave climate have been conducted, highlighting the respective features of wind-seas and swells using the data from voluntary observing ships (VOS) (*e.g.*, Gulev *et al.*, 2003; Gulev and Grigorieva, 2006), remote sensing (*e.g.*, Chen *et al.*, 2002; Jiang and Chen, 2013), and model hindcast (*e.g.*, Hanley *et al.*, 2010; Semedo *et al.*, 2011; Fan *et al.*, 2014). Each type of above data sources has its own advantages and disadvantages, but they are all useful tools in the studies of wave climate, about which a detailed review is made by Semedo *et al.* (2011, 2015). These studies have drawn many similar conclusions such as the distributions of wind-seas and swells and the swell prevalence in the open ocean.

Analyses of global or basin-scale wave climate mostly

---

* Corresponding author. E-mail: haoyujiang@cug.edu.cn

focus on the large-scale wave dynamics and features in the open ocean. In regional seas, many mesoscale effects or local factors, such as the coastal wind, shoaling, and limited fetches, will lead to the different results for the wind-sea and swell climates in enclosed seas and marginal seas from those in the open ocean. This is confirmed by the study of Semedo *et al.* (2015) which presented a detailed wind-sea and swell climatology in the Nordic Seas using downscaling ERA-40 reanalysis data.

The China Seas is a regional affected by the East Asia monsoon with northerly prevailing in the (boreal) winter and southerly prevailing in the summer, and it is affected by extratropical storms in the winter and tropical cyclones in the summer. The wave can be strong in this region (Huang *et al.*, 2008), thus, many studies have been conducted on the assessment of wave energy in the China Seas (*e.g.*, Zheng *et al.*, 2012, 2013; Wan *et al.*, 2015), and there are also many studies on the wave climate and wave extrema in this region (*e.g.*, Huang *et al.*, 2008; Li *et al.*, 2016; Liang *et al.*, 2016; He and Xu, 2016; He *et al.*, 2018). Wave parameters including significant wave height (SWH), mean wave period (MWP), and mean wave direction (MWD) were employed to describe the wave climate in this studies without separating wind-seas and swells. These three parameters can only give a limited description of the sea state (Semedo *et al.*, 2011) as two different sea states might have the same SWH, MWP, and MWD. The aim of this study is to present the climatology of wind-seas and swells in the China Seas, as analyzing the wind-sea and swell parameters separately can provide a more detailed description of the wave climate. There are no publicly available wave buoy data with more than 10 years' time series in the China Seas as far as we know. As for remote sensing data, altimetry cannot separate the wave energy from wind-seas and swells, and synthetic aperture radars still have some problems regarding the data quality to restrict its application to wave climate (Jiang *et al.*, 2017). The numerical wave model is still the best tool to investigate the wave climate of wind-seas and swells separately. Therefore, the Integrated Ocean Waves for Geophysical and other Applications (IOWAGA) dataset, which is a hindcast dataset of the numerical wave model WAVE-WATCH-III (WW3) (Tolman and the WAVE-WATCH-III Development Group, 2014), are employed in this study. The regional distribution of the wind-sea and swell wave parameters and their relation with the total wave parameters in the China Seas are presented.

The paper is organized as follows. The WW3 data employed in this study are briefly described and is validated against altimetry measurements in Section 2. The climatology of the wind-sea and swell parameters in the China Seas are presented in Section 3. The discussion and the concluding remarks are presented in Section 4.

2 Data and Methods

2.1 Model Data

IOWAGA dataset is the model hindcast outputs computed by WW3 with physical parameterizations of the source term package ST4 (Ardhuin *et al.*, 2010) forced by the global 10-m wind (U_{10}) data from the National Centers for Environmental Prediction (NCEP) Climate Forecast System Reanalysis (CFSR). The model simulation is performed at 0.5° spatial resolution and complemented by a multi-grid system including higher resolution up to 3′ in some focused regions, and unstructured grids are employed for the coastal domains (Rascle and Ardhuin, 2013). The directional spectrum computed in the model is spaced in 32 frequency bins, which increase exponentially from 0.038 to 0.72 Hz, and 24 directional bins with 15° spacing. The parameters of total wave fields such as total SWH and MWD employed in this study are integrated from the directional spectra. The spectrum at each grid is also partitioned into at most one wind-sea partition and up to five swell partitions using the method of Hanson and Philips (2001). For each partition, the SWH, peak wave period (PWP), and peak wave direction (PWD) can be obtained. Using the partition information, some other parameters such as the frequencies of occurrence of crossing sea or crossing swell (Jiang *et al.*, 2017) can be obtained. The outputs employed here are on a spatial resolution of 0.5°×0.5° and a temporal resolution of 3 h in the period of 1990–2016. This resolution is better for the studies of regional wave climate compared with other global hindcasts such as ERA-40 (Uppala *et al.*, 2005). It is noted that although contemporary numerical wave models are remarkably good in predicting windseas, they are still facing many problems regarding the reliability of swell prediction (*e.g.*, Young *et al.*, 2013; Stopa *et al.*, 2016b; Babanin and Jiang, 2017). In this model, an explicit swell dissipation source term is included for parameterizing based on the result of Ardhuin *et al.* (2009). Although the swell problem is not totally solved, the data shows good agreement with the observations from both buoys and altimeters (*e.g.*, Ardhuin *et al.*, 2010; Stopa *et al.*, 2016a), and some studies about the evolution of swells are conducted using this dataset (*e.g.*, Delpey *et al.*, 2010; Jiang *et al.*, 2016). The data is available from the FTP server of IFREMER (ftp.ifremer.fr) where more detailed information is available (Rascle and Ardhuin, 2013).

2.2 Validation

To demonstrate the errors of the model and evaluate the performance of the IOWAGA dataset in the China Seas, the forcing wind data from CFSR and the SWH data from the model output are compared with the corresponding measurements from altimeters in the region of interests. Altimeters can provide simultaneous measurements of sea surface wind speeds and SWHs. Particularly, the altimeter-derived SWHs are believed to have an accuracy comparable with in situ measurements (*e.g.*, Zieger *et al.*, 2009; Young *et al.*, 2017), and are widely used for verification and validation of numerical wave models (*e.g.*, Ardhuin *et al.*, 2010; Stopa *et al.*, 2016a). The altimeter dataset selected here is a merged and calibrated altimeter wind and wave database processed by the French ERS Processing and Archiving Facility (CERSAT) which merges the observations from a series of altimeter missions

(Queffeulou *et al.*, 2011). This dataset has been validated against *in situ* measurements and jointly calibrated via cross altimeter comparisons, thus, it can be regarded as homogeneous and consistent. Detailed information about this database is available at URL: http://tinyurl.com/kg7 kofg. In this study, the data from Topex-Poseidon, ERS-2, GFO, Jason-1, Envisat, Jason-2 in the period 2001-2010 are selected for the model validation.

The measurements of altimeters falling into the same spatio-temporal grid of the model output are averaged to smooth the altimetry measurements along the satellite tracks, and the data pairs from the altimeter and the model output are collocated. The scatter plots for the comparison are shown in Fig.1 where the color bars are on a logarithm scale with the data density in each $0.1 \times 0.1\,\mathrm{m\,s^{-1}}$ or $0.05\,\mathrm{m} \times 0.05\,\mathrm{m}$ bin. The bias, root mean square error (RMSE), and correlation coefficient (*R*) are computed. In the China Seas and their nearby waters (the spatial range for the comparison is shown in Fig.2), the bias of wind speed is $-0.32\,\mathrm{m\,s^{-1}}$, which means the wind speed is slightly underestimated in CFSR. The value of *R* for wind speed is 0.88 and the RMSE is 1.68. This result is in line with the comparison between CFSR and Envisat wind speed data made by Stopa *et al*. (2016a). The bias of SWH is -0.16 m, which means the model also tend to slightly underestimate the SWH. The two datasets are highly correlated

with a *R* of about 0.94 and the RMSE is about 0.37 m.

Fig.2a displays the spatial distributions of the bias of SWH and Fig.2b displays the distribution of RMSE of wind speeds from CFSR. Relatively large errors are mainly located in coastal regions, especially near the coasts of Taiwan, the Philippine Islands, and the Indonesian Archipelago. The corresponding bias and RMSE distribution maps of SWHs are displayed in Figs.2c and 2d. Similarly, relatively large errors of SWHs are also mainly located in coastal regions. Near the aforementioned regions with large errors of wind speeds such as Taiwan and the Philippine Islands, the errors of SWHs are also relatively large possibly due to the errors in the forcing wind field. The bias of SWHs is generally over -0.3 m and the RMSE is larger than 0.5 m in these regions. Another region with RMSE of SWHs larger than 0.5 m is the waters near the Ryukyu Islands, which might be mainly due to the insufficient sub-grid blocking and the lack of considering wave reflection/diffraction of islands in the numerical wave models. These regions significantly increase the overall errors in Fig.1, and except for these regions, most areas in the China Seas have a much lower error with the bias less than 0.2 m and the RMSE less than 0.3 m. In general, the SWHs from the model compare well with the observations and are sufficient to conduct studies of wave climate in the China Seas.
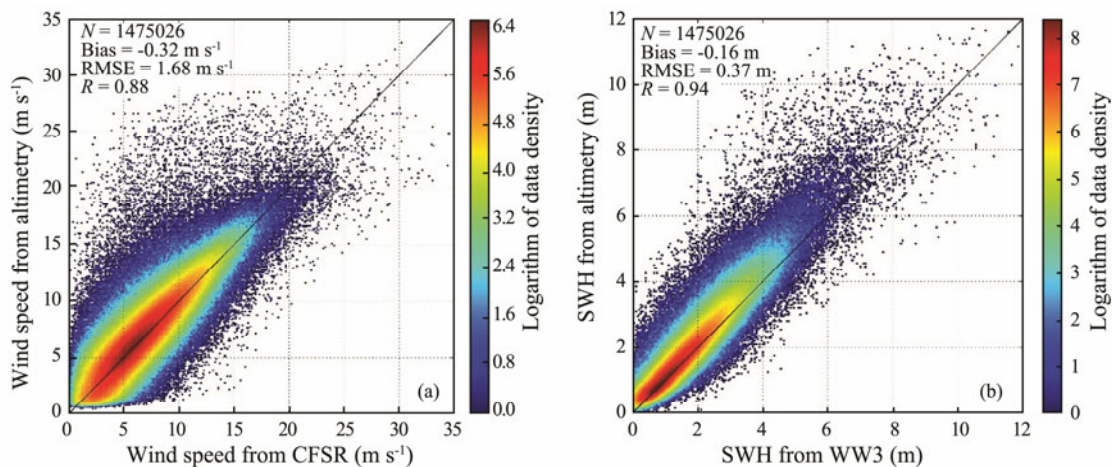

Fig.1 The scatter plots of collocated datasets in the China Seas and nearby waters from 2001 to 2010: (a) wind speeds from CFSR and (b) SWHs from WW3 hindcast versus corresponding measurements from altimeters. The data density is plotted on a logarithmic scale.

3 China Seas Wind-Sea and Swell Climates

All the data from the model are divided into four groups according to the seasonal partition of World Meteorological Society: boreal spring (March–May, MAM), summer (June–August, JJA), autumn (September–November, SON), and winter (December–February, DJF). Only the maps of extreme seasons, DJF and JJA, are visualized in the text in spite of some descri- ptions about MAM and SON. Both the mean wind and wave directions in the text are computed by averaging the zonal and meridional components separately. It is also noted that all the wind

and wave direction arrows in the maps are not scaled with the background field.

3.1 Wind-Sea and Swell SWHs

The climatological means of the U_{10} and wind direction (arrows) in the China Seas for DJF and JJA are shown in Fig.3. The seasonality of the surface wind field in this region, which is controlled by the monsoon, is noticeable in the figure. In winter, the mean U_{10} is higher than $8\,\mathrm{m\,s^{-1}}$ in most of the area of interest, and higher than $10\,\mathrm{m\,s^{-1}}$ in the Taiwan Strait, Luzon Strait, and to the southeast of Indo-China Peninsula. The region with the strongest mean wind speed is in the Taiwan Strait, and the sea with the
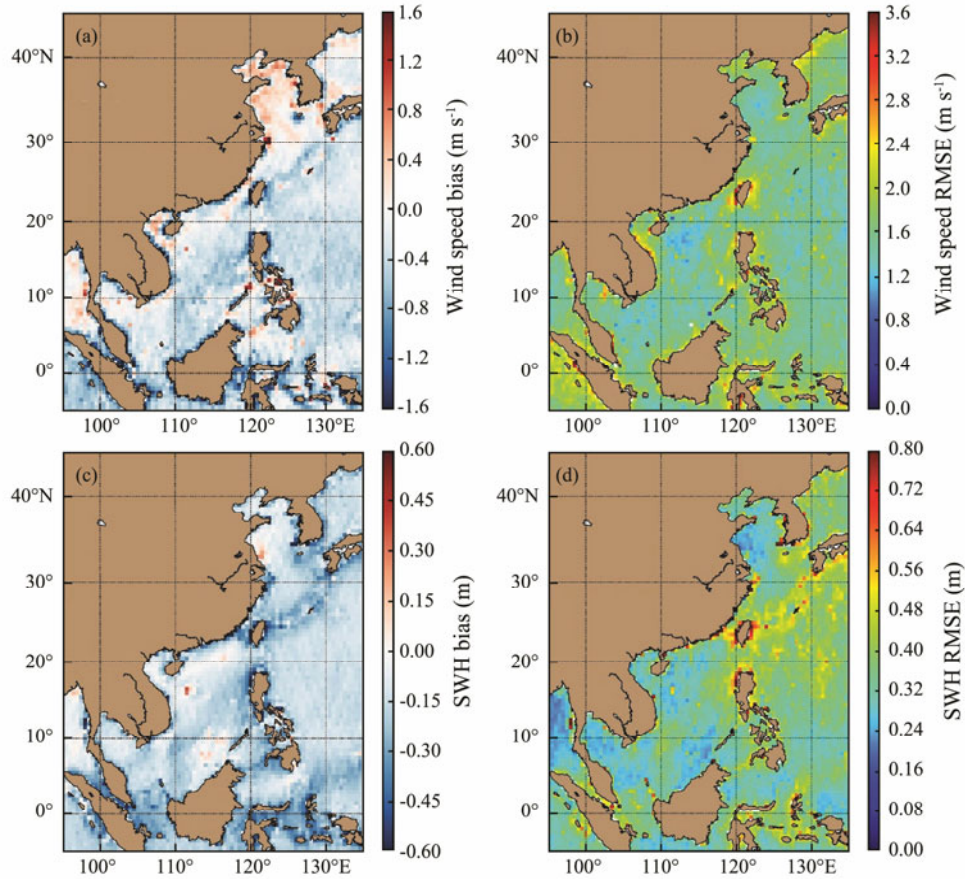
Fig.2 The spatial distributions of the errors presented as, (a) bias and (b) RMSE for wind speeds and (c) bias and (d) RMSE for SWHs, in the China Seas and nearby waters from 2001 to 2010.
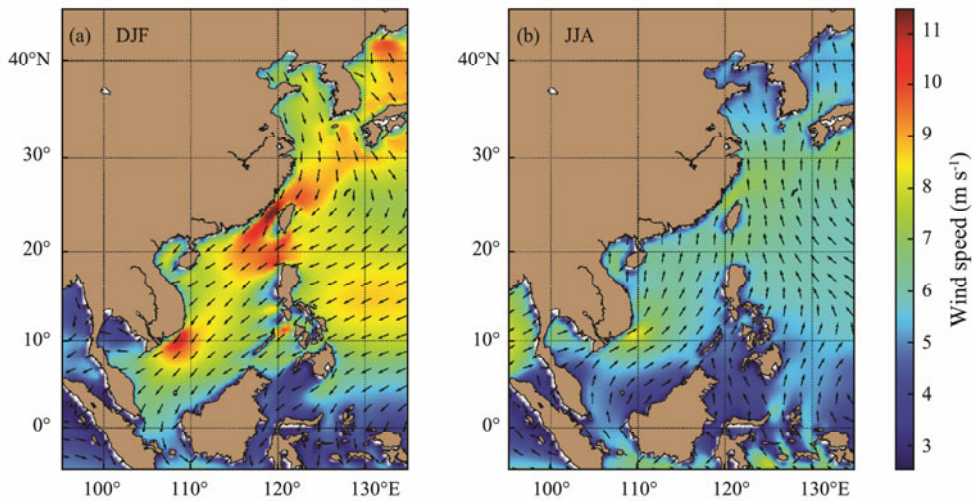

Fig.3 Seasonal averages of sea surface wind speed and wind direction in China Seas for (a) DJF and (b) JJA.

weakest wind is the Bohai Sea, where the wind speeds are still higher than $7\,\mathrm{m\,s^{-1}}$ in winter. In summer, the climatological means of U_{10} are generally lower than those in winter with values of around $6\,\mathrm{m\,s^{-1}}$ in most parts of the China Seas. The U_{10} in the Taiwan Strait, Luzon Strait, Ryukyu Islands waters can reach $7\,\mathrm{m\,s^{-1}}$, and the maximum U_{10} in summer is found to the southeast of Indo-China Peninsula (around $8\,\mathrm{m\,s^{-1}}$), which is due to the summer southwest monsoon. The surface winds are predominantly northerly

in the Bohai Sea, the Yellow Sea, and the East China Sea and are predominantly north-easterly in the South China Sea (SCS) during winter. During summer, the wind directions are opposite in the area of interest, being predominated by southerly and south-westerly. As the winds are stronger in winter, the distributions of wind directions in MAM and SON (not shown) are more close to those in DJF than JJA with the north-easterly predo- minant wind.

The seasonal maps of climatological mean SWH, wind-

sea SWH, and swell SWH for DJF and JJA in the China Seas are displayed in Fig.4. The arrows in the maps represent the averaged total/wind-sea/swell MWD over the period of interest. The two most noticeable features in the figure are 1) the similarity between the patterns of total wave fields and wind-sea fields and 2) that the mean wind-sea SWHs are generally higher than the mean swell SWHs, in both seasons. Previous studies have shown that the swell energy is much higher than the wind-sea energy in the open ocean from a climatological point of view (*e.g.*, Semedo *et al.*, 2011; Jiang and Chen, 2013). However, this is not the case in the regional seas like the China Seas where limited fetches make it hard for wind-seas to convert into swells and swells cannot propagate over large distances even if they can be generated. As wind-seas are strongly coupled with the local wind, the distributions of wind-seas are consistent with those of surface wind in respect of both intensity and direction. The wind-sea SWHs are higher in DJF than in JJA and the wind-sea MWDs are opposite in the two seasons.
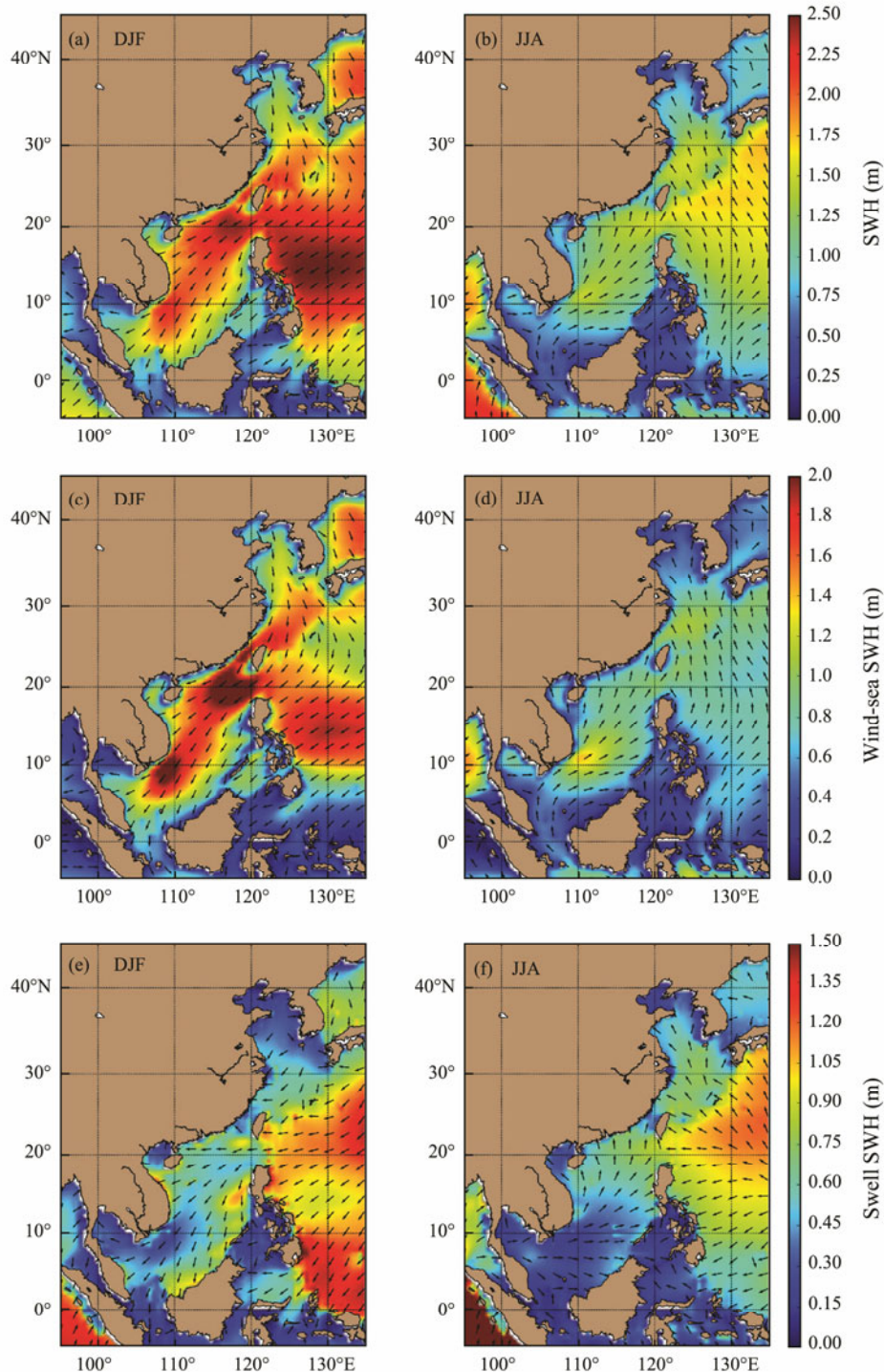

Fig.4 Distribution of seasonal averages of total SWHs and MWDs for (a) DJF and (b) JJA, wind-sea SWHs and MWDs for (c) DJF and (d) JJA, swell SWHs and MWDs for (e) DJF and (f) JJA in China Seas.

For swells, the situations are different in the SCS and the other three seas. The Bohai Sea is a small and shallow semi-enclosed sea so that the swells are weak in both DJF and JJA. Although the Ryukyu Islands can partially block the swells energy coming from the West Pacific leading to a clear boundary of swell SWHs between the East China Sea and the West Pacific, some swells from the West Pacific can still propagate into the East China Sea and the Yellow Sea. The swell climates in these two seas are the superposition of the westward swells from the West Pacific and the 'local swells' propagating southward in winter and northward in summer. Therefore, the total swell directions are generally southwestward in DJF and northwestward in JJA in these two seas. Sheltered by the islands around, few westward swells from the West Pacific can propagate into the SCS. Most swells in the SCS are 'local swells' which are residual waves of diminished wind and waves that have just propagated out of fetches, thus, the wave directions of swells and wind-seas are similar in the SCS. In the open ocean, the regions with large wind-sea energy are usually also regions with relatively large swell energy and vice versa. For instance, both wind-seas and swells are strong in the midlatitude storm track regions and generally weak in the tropical regions (Semedo et al., 2011). The condition can be different in regional seas. The SWHs of swells and wind-seas show somewhat opposite distributions in the SCS, which is particularly clear in JJA: the swells in the north of the SCS are from the northeastward wind-seas which propagate out of the fetches to the southeast of Indo-China Peninsula. In DJF, it can also be observed that most swells in the basin are located in areas around the central high-wind-sea areas. The results show that the local wind-sea and swell climates are mainly impacted by the orientation of fetches as well as the island sheltering, which is in line with the conclusions drawn by Semedo et al. (2015).

3.2 Wind-Sea and Swell Probabilities

The concept of wind-sea/swell probability presented by Chen et al. (2002) is widely used in the studies of wave climate. A binary classification to the sea states might be simplistic considering the complexity of the wave field, but it has been proved to be an effective and statistically meaningful description (e.g., Hanley et al., 2010; Semedo et al., 2011, 2015). The probability of swells and wind-seas at a given grid point can be calculated as $P_s=N_s/N$ and $P_w=N_w/N$, where N, N_s, and N_w are the numbers of total events, swell-dominated events, and wind-sea-dominated events, respectively. According to the definition, the sea state should be dominated by either wind-seas or swells, so that $P_s+P_w=1$.

Previous studies usually used the fully developed wind-wave relations, either the relation between wind speeds and SWHs (e.g., Chen et al., 2002; Jiang and Chen, 2013) or the relation between wind speeds and peak wave phase speeds (e.g., Hanley et al., 2010; Semedo et al., 2011, 2015), to determine whether the sea state is swell-dominated or wind-sea-dominated. For the cases that most of the wave energy is carried by the wave component with

the highest peak in the spectrum, these two categories of criteria are equivalent (Pierson, 1991). However, for a mixed sea state with two or more wave components with similar energy, these criteria might become somewhat inaccurate. For instance, when the sea state is dominated by nearly fully-developed wind-seas, an overlapped swell system with only half energy will let the total SWH exceed the threshold of the fully-developed SWH, leading to the sea state being regarded as a swell-dominated one. Therefore, these criteria are only regarded as valid from a statistical point of view (Chen et al., 2002). The partitioning of wave spectra (e.g., Hanson and Philips, 2001) makes the task of identifying the predominant wave much simpler since the SWHs of both wind-seas and swells can be obtained from the model output after spectral partitioning. If the swell energy is larger than the wind-sea energy at a given time and location, the sea state can be regarded as swell-dominated, otherwise, wind-sea-dominated. This definition can be used to diagnose the dominated wave component both case-by-case and statistically. In this study, the swell probability can then be simply defined as $P_s=P[H_s\geq H_w]$, where H_s denotes the swell SWH and H_w denotes the wind-sea SWH. Similarly, the wind-sea probability will be $P_w=P[H_s<H_w]=1-P_w$.

Chen et al. (2002) have shown that the swell probability is more than 75% in most areas of the open ocean, even in the mid-latitude areas where strong wind-waves are generated, and this number can reach 100% in the tropical 'swell pools'. Follow-on studies (e.g., Hanley et al., 2010; Semedo et al., 2011; Jiang and Chen, 2013) also confirmed these results. The spatial distributions of wind-sea probabilities in the China Seas for DJF and JJA are shown in Fig.5. The distributions of swell probability, which are totally opposite to that of wind-sea, are not shown in order to save space. One of the most noticeable features in Fig.5 is the predominance of wind-seas in the China Seas. The wind-sea probability is more than 75% in most parts of the China Seas in DJF, and is generally lower in JJA, but it is still more than 50% in most areas of interests. In both seasons, the highest probability of occurrence of wind-sea-dominated wave field is found to the southeast of Indo-China Peninsula, which is due to the outbreak of monsoon. In MAM and SON (not shown), this region also has high wind-sea probabilities, but not as high as in DJF and JJA. The Taiwan Strait has the wind-sea probability of nearly 90% in DJF and of about 80% in MAM and SON due to the local high wind speeds. Other regions with high wind-sea probability can be found in the Beibu Gulf and the Bohai Sea where the fetch length is very low and swells can hardly intrude. Lower wind-sea predominance is found in the leeside of the Luzon Island and the northeast coasts of Kalimantan Island in DJF, which can be linked with the low wind speeds in these regions as shown in Fig.3a. In JJA, the wind-sea predominance is also notably low in the Yellow Sea and the northeast of the SCS, with wind-sea probabilities of less than 50%, which can roughly be linked with the wind-sea and swell SWH patterns in Figs.4d and 4f.

In both two regions where swell probabilities are rela-

tively high (the Yellow Sea and the northeast of the SCS), the swells from the West Pacific contributes signi- ficantly to the swell predominance. This can be confirmed by plotting the map of crossing swell probability in JJA (not shown) using the scheme of Jiang *et al.* (2017). It is found that both these two regions have the crossing swell probability of more than 30%, showing that the energy of the 'local swells' and the 'extraneous swells' are often comparable with each other. Using the partitioned wave spectrum, the wave PWP and SWH roses at the point 20˚N, 120˚E for JJA representing the occurrence of wave events per direction are plotted in Fig.6 as an example. There are clearly two sets of wave systems with different directions, a westward one and a northeastward one. Limited by the fetch and the propagation distance, the PWPs of the

northeastward waves at this point, even for swells, can hardly reach 10 s. Meanwhile, nearly half of the westward waves (mainly swells coming from the West Pacific) have the PWP of more than 10 s and can reach 20 s. The frequencies of occurrences of the westward swell events are also generally higher than the northeastward ones. However, the swells from the West Pacific are mostly generated thousands of kilometers away, and their energies have been attenuated by frequency dispersion, angular spreading, and dissipation. Therefore, most of the swells propagating westward in the SCS only have an SWH of less than 0.5 m, while the northeastward waves have much more energy. That is why the MWDs of both wind-sea and swells in JJA are northeastward at this point, even if the swells from West Pacific are non-negligible.
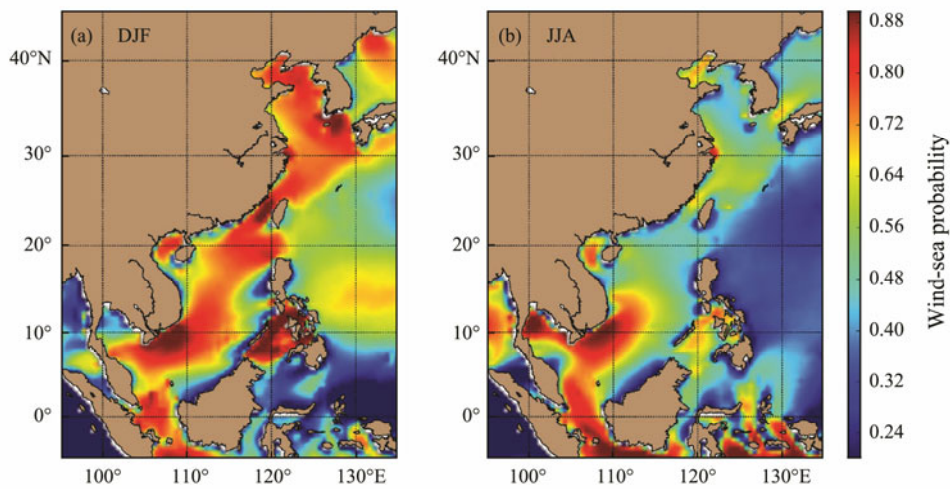

Fig.5 Seasonal distributions of wind-sea probability in China Seas for (a) DJF and (b) JJA.
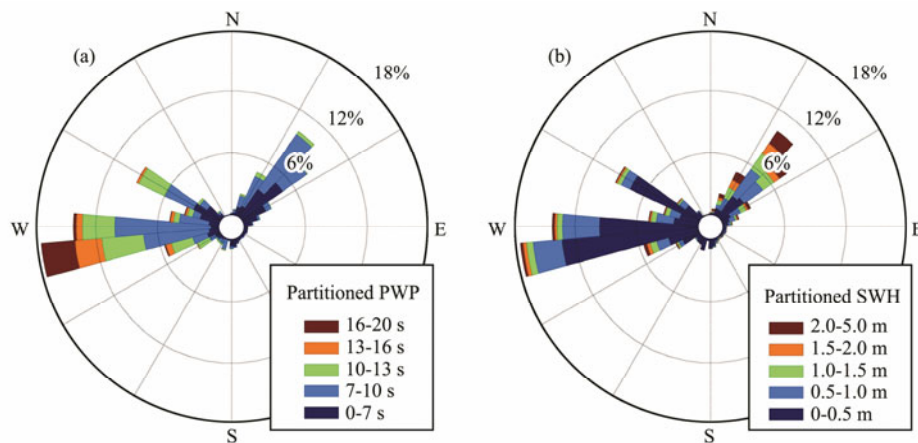

Fig.6 Wave rose plots of (a) partitioned PWD and (b) partitioned SWH at 20˚N, 120˚E for JJA. The direction of the sector denotes the direction that waves propagate towards.

3.3 Wind-Sea and Swell Energy Proportions

Fig.4 shows that the wind-sea SWHs are larger than the swell SWHs in most areas of interests in the China Seas, and Fig.5 shows that the wind-seas are also more prevalent than swells in respect of time in the China Seas. To estimate the relative weights of wind-seas and swells in respect of energy, the energy densities per unit area in the

China Seas were computed for both wind-seas and swells following the method of Semedo *et al.* (2011, 2015). The energy proportions of wind-seas and swells to the total wave energy are then computed and are displayed in Fig.7 (only the energy proportion of wind-seas is shown as that of swells is simply opposite). Not surprisingly, in spite of the different definitions, there are many similarities between the distributions of wind-sea probability and

wind-sea proportion. For instance, the southeast of Indo-China Peninsula has high wind-sea energy proportions in both seasons. Areas with the lowest wind-sea energy proportions are located in the leeside of the Luzon Island and the northeast coasts of Kalimantan Island in DJF. However, it is clear that the wind-sea proportions are significantly higher than the wind-sea probabilities over the areas of interests (the color bars in Fig.5 and Fig.7 are the

same). By spatially averaging the data of the China Seas in Fig.7, it is found that more than 90% of the wave energy at the surface of the China Seas in DJF and more than 75% in JJA are wind-sea energy. Even in the Yellow Sea and the northeast of the SCS where the wind-sea probabilities are less than 50%, the wind-seas in JJA can still contribute more than 50% of the wave energy to the wave fields from a climatological point of view.
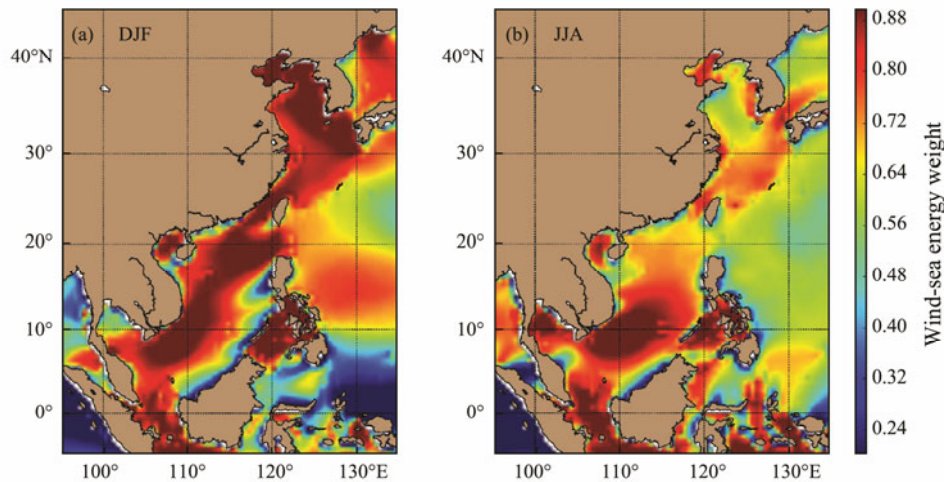

Fig.7 Seasonal distributions of wind-sea energy weight in China Seas for (a) DJF and (b) JJA.

On average, the wave energy during wind-sea-dominated events are higher than during swell-dominated events, as extreme sea states are more linked with wind-seas. For instance, Huang *et al.* (2008) pointed out the response of summertime extreme wave heights to local wind climate in the East China Sea. This can explain why the wind-sea energy proportion is systematically higher than the wind-sea probability at a given position from a climatological point of view. To demonstrate this phenomenon, the distributions of maximum SWHs for DJF and JJA in 2000 are shown in Fig.8 along with the corresponding wind-sea and swell SWHs. Extreme SWHs in China Seas are usually due to severe meteorological events such as extratropical storms in the winter and tropical cyclones in the summer. For instance, a typhoon event (BILIS, No. 200010) can be observed with SWHs of more than 8 m along the track in Fig.8b. Such spatial distributions of maximum SWHs are also plotted for other years and seasons (not shown). Although the spatial patterns of the maximum SWHs are different from season to season, they always have much higher consistency with the spatial patterns of the corresponding wind-sea SWHs than swell SWHs. This indicates that wind-seas are over-whelmingly predominated in such extreme sea states. In contrast, the swell-dominated events usually correspond to relatively low total SWHs. Therefore, even in the situation that the probabilities of wind-seas and swells are similar, wind-sea SWHs will have higher climatological mean than swell SWHs. Such a phenomenon can also be observed in the open ocean. The swell probabilities are also slightly higher than the swell energy proportions in the global ocean according to Fig.4 and Fig.6 of Semedo *et al.* (2011), indicating that

the method of using the swell/ wind-sea probabilities to approximate the swell/wind-sea proportions presented by Jiang and Chen (2013) will lead to systematic errors and needs to be improved.

4 Discussion and Conclusions

The wave climatology in the China Seas is presented using the IOWAGA hindcast data from 1990–2016 in this study. The wind-seas and swells are analyzed separately considering the fact that the wave parameters integrated from the entire wave spectrum such as the total SWH might only give a limited description of the wave field. A multiple-source altimetry dataset of wind speeds and SWHs is employed to validate the performance of the WW3 model and the result confirms that the WW3 outputs employed in this study are sufficient for studies of wave climates in the China Seas.

The characteristics of wind-seas and swells in the China Seas are very different from those in the open ocean where swells dominate the sea states. In most areas of the China Seas, the SWH of wind-seas is significantly higher than that of swells and the wind-seas are predominant. On the one hand, wind-seas require sufficient time and space to grow into large swells and propagate away from their generation areas, but the limited fetches in the China Seas make the waves hard to reach a fully-developed state and to turn into swells. On the other hand, the islands around the China Seas shelter most of the swells from the West Pacific. Most of the swells in the China Seas are relatively short-wavelength 'local swells' which have just propagated out of their fetches. These
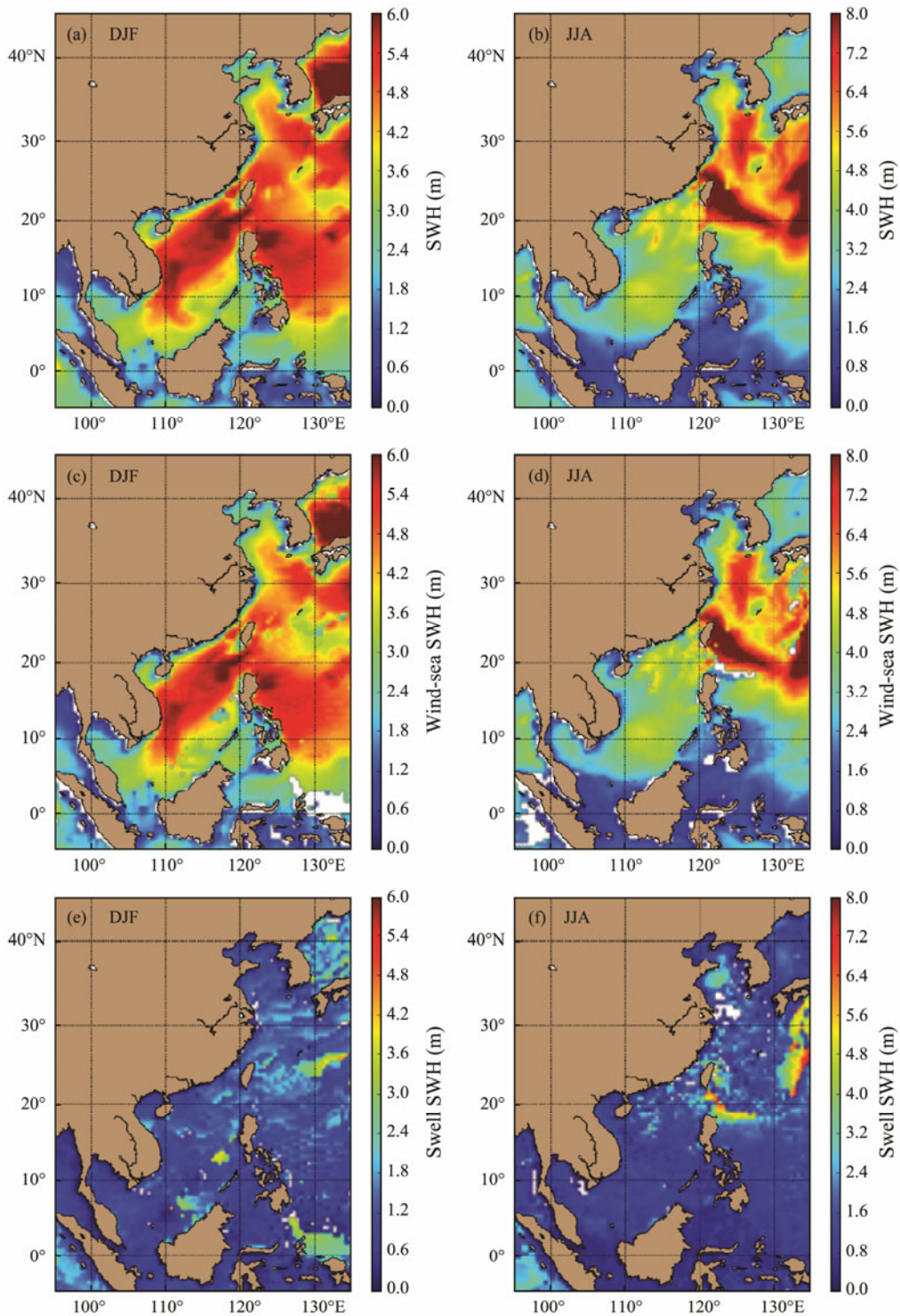
Fig.8 Distributions of maximum SWHs for (a) DJF and (b) JJA and the corresponding wind-sea SWHs ((c) and (d)) and swell SWHs ((e) and (f)) in 2000 in the China Seas.

features can also be found in other enclosed and semi- en- closed seas where the geometry of the coasts is an im- portant factor to influence the wind-sea and swell climate. In the winter of the China Seas, the relatively stronger norther corresponds to a longer fetch for the fully- developed sea state so that the predominance of wind- seas is more obvious than in the summer when the swell probabilities can be more than 50% in some parts of the areas of interests. However, even in the waters where the

swell probabilities are more than 50%, the energy weights of swells may be less than 50%. The energy weights of wind-seas are generally higher than the wind-sea pro- babilities in a given location because wind-sea-domina- ted events usually have higher energy than swell-domi- nated events and most extreme wave events with high SWHs are related to wind-sea conditions.

The results of this study confirmed that the study separating wind-seas and swells can give a much more

detailed description of the wave climate. However, based on the spectrum partitioning scheme, it is found that there might be more than two systems of swell climates with distinct wave directions and wave periods at a given location as shown in Fig.6. So only the classification of wind-seas and swells might be still insufficient. The wave rose can reveal the detailed swell climate at a fixed point, but more advanced methods or technologies are still needed to describe the spatial patterns of swell climates especially in the crossing swell conditions. The wave climate is a very important part of the global climate system. The long-term variability of the wave parameters for wind-sea and swells in the China Seas and the relation between the interannual variability of wave climates and the El Niño/ Southern Oscillation are not discussed here as the time series of the dataset used in this study does not reach the minimum length of 30 years recommended by the World Meteorological Organization. Further studies on the long-term and interannual variability of wind-sea and swell climates could be conducted by using wave hindcasts with a longer time span.

Acknowledgements

References

Ardhuin, F., Chapron, B., and Collard, F., 2009. Observation of swell dissipation across oceans. *Geophysical Research Letters*, **36**: L06607, DOI: 10.1029/2008GL037030.

Ardhuin, F., Rogers, E., Babanin, A., Filipot, J., Magne, R., Roland, A., Van der Westhuysen, A., Queffeulou, P., Lefevre, J., Aouf, L., and Collard, F., 2010. Semi-empirical dissipation source functions for ocean wave. Part I: Definition, cali- bra- tion and validation. *Journal of Physical Oceanography*, **40**: 1917-1941.

Babanin, A. V., and Jiang, H., 2017. Ocean swell, how much do we know. *Processing 36th International Conference on Ocean, Offshore and Arctic Engineering*, Trondheim, DOI: 10.1115/ OMAE2017-61692.

Chen, G., Chapron, B., Ezraty, R., and Vandemark, D., 2002. A global view of swell and wind sea climate in the ocean by satellite altimeter and scatterometer. *Journal of Atmospheric and Oceanic Technology*, **19**: 1849-1859.

Delpey, M. T., Ardhuin, F., Collard, F., and Chapron, B., 2010. Space-time structure of long ocean swell fields. *Journal of Geophysical Research*, **115**: C12037, DOI: 10.1029/2009JC 005885.

Drennan, W. M., Graber, H. C., Hauser, D., and Quentin, C.,

2003. On the wave age dependence of wind stress over pure wind seas. *Journal of Geophysical Research*, **108**: 8062, DOI: 10.1029/2000JC000715.

Fan, Y., Lin, S., Griffies, S., and Hemer, M., 2014. Simulated global swell and wind-sea climate and their responses to anthropogenic climate change at the end of the twenty-first century. *Journal of Climate*, **27**: 3516-3536.

Gulev, S. K., and Grigorieva, V., 2006. Variability of the winter wind waves and swell in the North Atlantic and North Pacific as revealed by the voluntary observing ship data. *Journal of Climate*, **19**: 5667-5685.

Gulev, S. K., Grigorieva, V., Sterl, A., and Woolf, D., 2003. Assessment of the reliability of wave observations from voluntary observing ships: Insights from the validation of a global wind wave climatology based on voluntary observing ship data. *Journal of Geophysical Research*, **108**: 3236-3236.

Hanley, K. E., Belcher, S. E., and Sullivan, P. P., 2010. A global climatology of wind-wave interaction. *Journal of Physical Oceanography*, **40**: 1263-1282.

Hanson, J. L., and Phillips, O. M., 2001. Automated analysis of ocean surface directional wave spectra. *Journal of Atmospheric and Oceanic Technology*, **18**: 277-293.

He, H., and Xu, Y., 2016. Wind-wave hindcast in the Yellow Sea and the Bohai Sea from the year 1988 to 2002. *Acta Oceanologica Sinica*, **35**: 46-53.

He, H., Song, J., Bai, Y., Xu, Y., Wang, J., and Bi, F., 2018. Climate and extrema of ocean waves in the East China Sea. *Science China－Earth Sciences*, **61** (7): 980-994, DOI: 10.10 07/s11430-017-9156-7.

Huang, Y., Yin, B., William, P., and Hou, Y., 2008. Responses of summertime extreme wave heights to local climate variations in the East China Sea. *Journal of Geophysical Research*, **113**: C09031, DOI: 10.1029/2008JC004732.

Janssen, P. A. E. M., 1989. Wave-induced stress and the drag of air flow over sea waves. *Journal of Physical Oceanography*, **19**: 745-754.

Jiang, H., and Chen, G., 2013. A global view on the swell and wind sea climate by Jason-1 mission: A revisit. *Journal of Atmospheric and Oceanic Technology*, **30**: 1833-1841.

Jiang, H., Mouche, A., Wang, H., Babanin, A. V., Chapron, B., and Chen, G., 2017. Limitation of SAR quasi-linear inversion data on swell climate: An example of global crossing swells. *Remote Sensing*, **9** (2): 107, DOI: 10.3390/rs9020107.

Jiang, H., Stopa, J. E., Wang, H., Husson, R., Mouche, A., Chapron, B., and Chen, G., 2016. Tracking the attenuation and nonbreaking dissipation of swells using altimeters. *Journal of Geophysical Research: Oceans*, **121**: 1446-1458, DOI: 10.10 02/2015JC011536.

Kinsman, B., 1965. *Wind Wave*. Prentice-Hall, New Jersey, 1- 676.

Li, J., Chen, Y., and Pan, S., 2016. Modelling of extreme wave climate in China Seas. *Journal of Coastal Research*, **32**: 522- 526.

Liang, B., Liu, X., Li, H., Wu, Y., and Lee, D., 2016. Wave climate hindcasts for the Bohai Sea, Yellow Sea, and East China Sea. *Journal of Coastal Research*, **32**: 172-180.

Pierson, W. J., 1991. Comment on 'effects of sea maturity on satellite altimeter measurements' by Roman E. Glazman and Stuart H. Pilorz. *Journal of Geophysical Research*, **96**: 4973- 4977.

Queffeulou, P., Ardhuin, F., and Lefèvre, J. M., 2011. Wave height measurements from altimeters: Validation status and applications. *OSTST Meeting, Ocean Surface Topography Science Team*. San Diego, 19-21.

Rascle, N., and Ardhuin, F., 2013. A global wave parameter database for geophysical applications. Part 2: Model validation with improved source term parameterization. *Ocean Modelling*, **70**: 174-188.

Semedo, A., Sušelj, K., Rutgersson, A., and Sterl, A., 2011. A global view on the wind sea and swell climate and variability from ERA-40. *Journal of Climate*, **24**: 1461-1479.

Semedo, A., Vettor, R., Breivik, Ø., Sterl, A., Reistad, M., and Lima, D., 2015. The wind sea and swell waves climate in the Nordic Seas. *Ocean Dynamics*, **65**: 233-240, DOI: 10.1007/s10236-014-0788-4.

Stopa, J. E., Ardhuin, F., Bababin, A. V., and Zieger, S., 2016a. Comparison and validation of physical wave parameterizations in spectral wave models. *Ocean Modelling*, **103**: 2-17, DOI: 10.1016/j.ocemod.2015.09.003.

Stopa, J. E., Ardhuin, F., Husson, R., Jiang, H., Chapron, B., and Collard, F., 2016b. Swell dissipation from 10 years of Envisat advanced synthetic aperture radar in wave mode. *Geophysical Research Letters*, **43** (7): 3423-3430.

Tolman, H. L., and the WAVEWATCH III® Development Group, 2014. User manual and system documentation of WAVE-WATCH III® version 4.18. Technical Note 316. NOAA/NWS/NCEP/MMAB, U. S. Department of Commerce, National Oceanic and Atmospheric Administration, College Park, Md, 1-282.

Uppala, S. M., Kållberg, P. W., Simmons, A. J., Andrae, U., Bechtold, V. D. C., Fiorino, M., Gibson, J. K., Haseler, J., Hernandez, A., Kelly, G. A., Li, X., Onogi, K., Saarinen, S., Sokka, N., Allan, R. P., Andersson, E., Arpe, K., Balmaseda, M. A., Beljaars, A. C. M., Van De Berg, L., Bidlot, J., Bormann, N., Caires, S., Chevallier, F., Dethof, A., Dragosavac, M., Fisher, M., Fuentes, M., Hagemann, S., Hólm, E., Hoskins, B. J., Isaksen, L., Janssen, P. A. E. M., Jenne, R., McNally, A. P., Mahfouf, J. F., Morcrette, J. J., Rayner, N. A., Saunders, R. W., Simon, P., Sterl, A., Trenberth, K. E., Untch, A., Vasiljevic, D., Viterbo, P., and Woollen, J., 2005. The ERA-40 re-analysis. *Quarterly Journal of the Royal Meteo- rological Society*, **131**: 2961-3012.

Wan, Y., Zhang, J., Meng, J., and Wang, J., 2015. A wave energy resource assessment in the China's seas based on multi-satellite merged radar altimeter data. *Acta Oceanologica Sinica*, **34**: 115-124.

Young, I. R., Babanin, A. V., and Zieger, S., 2013. The decay rate of ocean swell observed by altimeter. *Journal of Physical Oceanography*, **43**: 2322-2333.

Young, I. R., Sanina, E., and Babanin, A. V., 2017. Calibration and cross validation of a global wind and wave database of altimeter, radiometer, and scatterometer measurements. *Journal of Atmospheric and Oceanic Technology*, **34** (6): 1285-1306, DOI: 10.1175/JTECH-D-16-0145.1.

Zheng, C., Pan, J., and Li, J., 2013. Assessing the China Sea wind energy and wave energy resources from 1988 to 2009. *Ocean Engineering*, **65**: 39-48.

Zheng, C., Zhuang, H., Li, X., and Li, X., 2012. Wind energy and wave energy resources assessment in the East China Sea and South China Sea. *Science China－Technological Sciences*, **55**: 163-173.

Zieger, S., Vinoth, J., and Young, I. R., 2009. Joint calibration of multiplatform altimeter measurements of wind speed and wave height over the past 20 Years. *Journal of Atmospheric and Oceanic Technology*, **26**: 2549-2564.

(Edited by Chen Wenwen)